Colloidal II–VI-Epitaxial III–V heterostructure: A strategy to expand InGaAs spectral response

Adrien Khalili, Claire Abadie, Tung Huu Dang, Audrey Chu, Eva Izquierdo, Corentin Dabard, Charlie Gréboval, Mariarosa Cavallo, Huichen Zhang, Stefano Pierini, et al.

Colloidal II-VI - epitaxial III-V heterostructure: a strategy to expand InGaAs spectral response

Adrien Khalili[1], Claire Abadie[2], Tung Huu Dang[1], Audrey Chu[1], Eva Izquierdo[1], Corentin Dabard[1,3], Charlie Gréboval[1], Mariarosa Cavallo[1], Huichen Zhang[1], Stefano Pierini[1], Yoann Prado[1], Xiang Zhen Xu[3], Sandrine Ithurria[3], Grégory Vincent[2], Christophe Coinon[4], Ludovic Desplanque[4], Emmanuel Lhuillier[1*]

[1]Sorbonne Université, CNRS - UMR 7588, Institut des NanoSciences de Paris, INSP, F-75005 Paris, France
[2]ONERA - The French Aerospace Lab, 6, chemin de la Vauve aux Granges, BP 80100, 91123 Palaiseau, France.
[3] Laboratoire de Physique et d'Etude des Matériaux, ESPCI-Paris, PSL Research University, Sorbonne Université Univ Paris 06, CNRS UMR 8213, 10 rue Vauquelin 75005 Paris, France.
[4]Univ. Lille, CNRS, Centrale Lille, Univ. Polytechnique Hauts-de-France, Junia, UMR 8520 - IEMN, F-59000 Lille, France

Abstract: For short wave infrared (SWIR) sensing, InGaAs is the leading technology combining high carrier mobility, high homogeneity and complete control over *n*-to-*p* doping. In the meanwhile, numerous alternative materials have tried to compete with InGaAs. Among them, colloidal nanocrystals with narrow band gap can address the current issue in designing cost-effective sensors for the SWIR range. Rather than pitting these two materials against each other, here we design a synergistic duo in which HgTe nanocrystals are used to broaden the spectral range of InGaAs while lifting the lattice matching constraints. We propose a diode geometry where a *p*-type HgTe NC array is coupled with *n*-type InGaAs wires which are used as high mobility (μ>1000 $cm^2.V^{-1}s^{-1}$) minority carrier extractors. This approach also demonstrates that Van der Waals heterostructures are not limited to graphene-like materials and that bulk-like III-V semiconductors can also be light sensitized by colloidal nanoparticles. This work paves the way toward further synergies between epitaxially grown and colloidally grown semiconductors for infrared detection.

*To whom correspondence should be sent: el@insp.upmc.fr

Wide band gap nanocrystals (NCs) with optical features in the visible are now commercially used as down-converters for displays. For narrow band gap NCs, it is rather their absorption properties that draw attention. They have been used to absorb the infrared (IR) tail of the solar spectrum in solar cells[1] or to design infrared cameras.[2–5] In the latter case NCs are often promoted as cost-effective alternatives to existing technologies that are heavily relying on epitaxially grown semiconductors. In the short-wave infrared range (SWIR), InGaAs technology[6] is certainly the most effective, combining high external quantum efficiency (EQE), low noise and a high uniformity. This causes historical and emerging technologies to often compete with each other.

Here, we demonstrate synergistic properties resulting from an InGaAs wire array[7] epitaxially grown coupled to an array of colloidal HgTe NCs. NCs being synthetized in solution, they are completely released from lattice-mismatched constraints with the substrate, which considerably eases the spectral tunability. On the other hand, InGaAs epitaxially obtained presents a high crystallinity leading to high carrier mobilities as well as a careful control of the doping. Here, we design and fabricate a diode structure where the InGaAs wires are used as electron extractors to form a *p-n* junction at the interface with the overall p-type HgTe NCs. Introduction of wires and rods as carrier extractors is a strategy already reported for solar cells and detectors. These examples are mainly based on ZnO and TiO_2 wires generally obtained from solution growth methods and are used to form bulk heterojunctions.[8,9] However, in the specific case of short wave infrared absorbing device, the band alignment of such wide band gap oxide appears suboptimal since it has been proven that the photocurrent is also filtered by the oxide layer, leading to very small device responsivity.[10] Thus, alternative material presenting more favorable band alignment have to be tested. Here, we use high mobility epitaxially grown nanowires with a band gap suited for IR sensing.

Recently, the combination of 1D wires with a matrix of a second material has been generalized under the concept of mixed dimensional van der Waals heterostructures.[11] The idea was initially proposed for 2D materials such as graphene and transition metal dichalcogenides[12,13] (TMDCs), but rapidly it appeared that such 2D materials could be functionalized by molecules,[14] nanoparticles[15,16] or even bulk materials.[17] Beyond their remarkable mechanical and electrical properties, the ease of functionalization of the 2D materials has become one of their most striking properties. However, these 2D materials also suffer from clear limitations: the graphene has no gap and the flake size of TMDC (few tens of µm) hinders the design of large-scale devices. These challenges (material stability, high mobility, doping control, large scale processing…) can easily be overcome using the high maturity of Silicon[18] or III-V semiconductors, while their coupling to nanoparticles remains mostly unexplored. Here, we demonstrate synergistic properties resulting from the III-V wire array and the II-VI NCs. In particular, we show that the spectral response of the hybrid structure can handily be designed to absorb longer wavelengths than the cut-off of bulk InGaAs. We also show that our strategy seamlessly leads to the formation of a *p-n* junction with a strongly rectifying I-V curve while such design relies on the complex choice of the surface chemistry and the coupling to carrier transport layers for all NC-based photodiodes.[19–21]

We start by growing an array of InGaAs nanowires. To do so, we use an InP substrate that is coated with silica by plasma enhanced chemical vapor deposition (Figure S1a). Then, the latter is patterned using e-beam lithography to define some openings down to the InP substrate (Figure S1b). This functionalized substrate is then introduced into a molecular beam epitaxy chamber to conduct the in-plane wires selective area growth (Figure S1c). We obtain an array of 200 wires which are 20 µm long and 130 nm wide. Various spacings (500, 700 and 1000 nm) between wires have been tested, though the results in the paper focus on the smallest period. To minimize the array resistance, a few perpendicular wires have also been included, see optical (**Figure 1**a) and electron microscopy image (**Figure 1**b and c). The wires are n-doped with a doping at 3.5×10^{18} cm^{-3}.

Then, we deposit metal contact electrodes to define the diode area (Figure S1d). One electrode overlaps with the wire array, while the second one is not contacted to the III-V semiconductor. Then

the device is coated with an HgTe NC array that is spread all over the surface. To ensure that the charge transport goes through the wire array, the metallic electrode is further insulated by a silica patch (purple area in the false color microscopy image, see Figure S1e and **Figure 1**a) which role is to prevent conduction in the NC array only. Finally, we grow HgTe NCs[22] using the procedure developed by Keuleyan *et al*.[23] The size of the particle (≈8 nm) is chosen so that their band edge (2 µm cut-off) is redder than the one of the InGaAs (1.6 µm cut-off). The absorption and photoluminescence (PL) spectra of the material are shown in **Figure 1**d. The band gap, determined at the maximum of the PL signal, is at 1.75 µm (≈700 meV) while the cut-off wavelength reaches ≈2 µm after ligand exchange to make the film conductive. The film of HgTe NC presents a 200-400 nm thickness (Figure S1f).

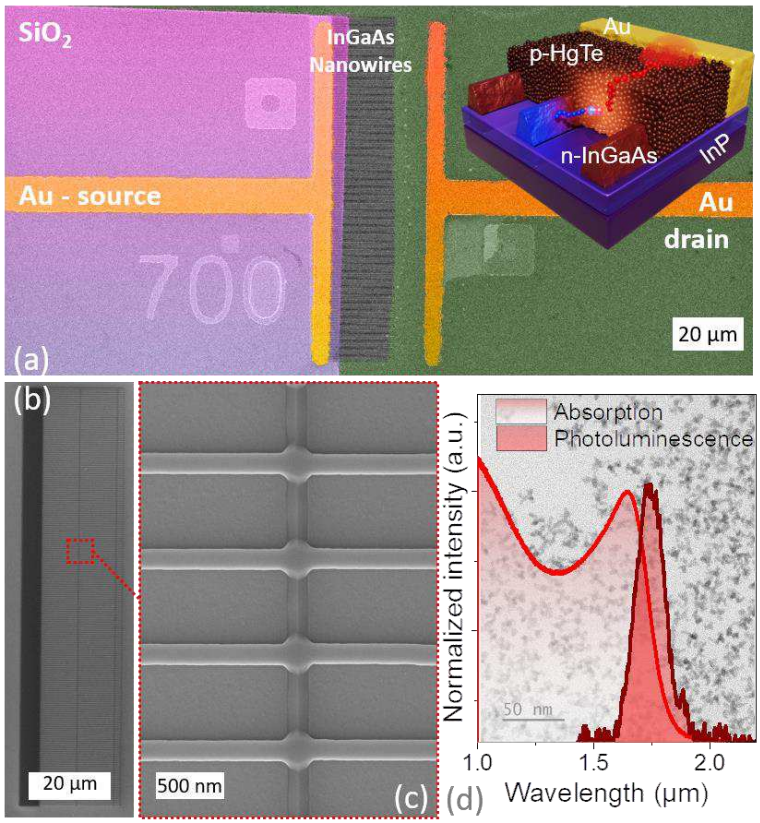

***Figure 1 InGaAs wires/HgTe NCs hybrid device**. a. False color microscopy image of the patterned nanowires. As a convention the wires are connected to the source in the following of the paper. The right side inset is a shematic of the device once coated by a HgTe NCs film. b. SEM image of the InGaAs wires array. c. Zoom on the InGaAs wires array. d. Normalized absorption and photoluminescence spectra of HgTe NCs. The background is a TEM image of the same HgTe NCs.*

Before discussing the transport and photo-transport properties of the hybrid structure, we characterized the conduction properties of the two materials independently. In order to probe the conduction in the wire only, a dedicated device where the wires are connected on both ends has been prepared. Due to their highly n-doped nature, the InGaAs wires only present a weak temperature dependence. The drop of the resistance upon cooling, see **Figure 2**a, can be attributed

to the increase in the electron mobility as the phonon scattering is reduced. I-V curve reveals an ohmic behavior (**Figure 2**b) while the Hall mobility is found to be ≈3000 $cm^2.V^{-1}s^{-1}$. By gating the wires array with an electrolyte, we confirmed that conduction rises under electron injection, see the inset of **Figure 2**b. The transport in the HgTe NC array is also associated with an ohmic behavior, consistent with a limited offset of the material with the gold electrode, see **Figure 2**d. Field effect measurement reveals conduction only by holes, see the inset of **Figure 2**d. This is related to the localization of the Fermi level in the bottom part of the band gap as revealed by photoemission for this HgTe NC size.[4] The temperature dependence of the current **Figure 2**c) is consistent with a thermally activated transport. The activation energy of the current is found to be ≈220 meV, which is slightly smaller than the half band gap value ($E_G/2$=350 meV) expected for an intrinsic semiconductor with the same band gap.

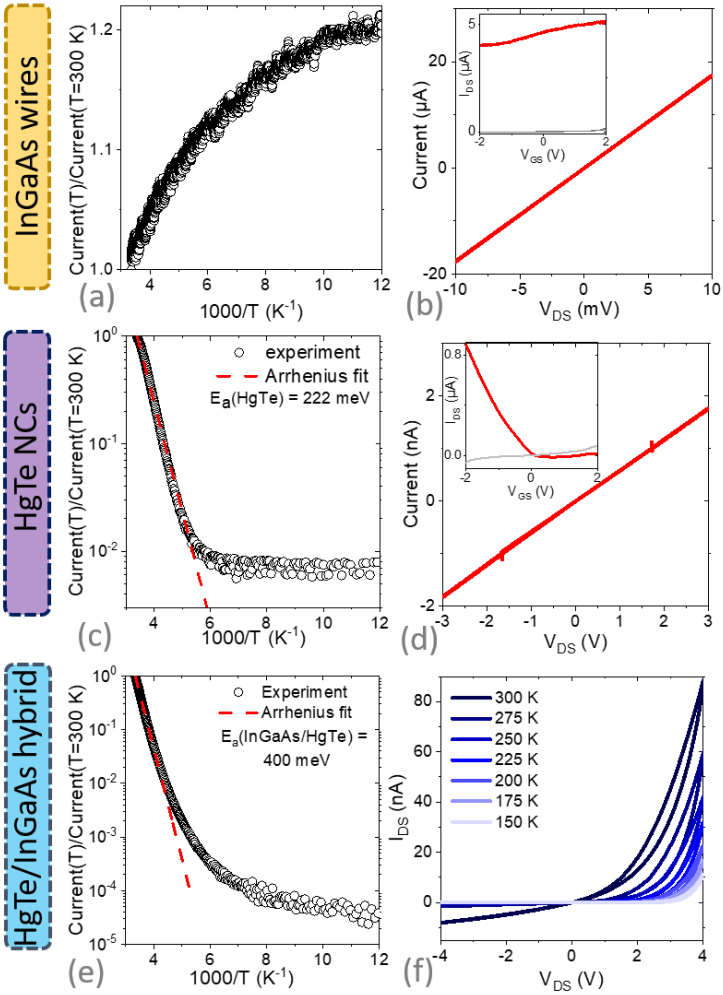

Figure 2 Transport properties of the InGaAs wires array, of the HgTe NCs array and of the hybrid structure*. a. Current (V_{DS}=1 mV) normalized by its value at room temperature as a function of the temperature for an array of InGaAs wires connected on both ends. b . Dark I-V curve, at room temperature, for the InGaAs wires array. The inset is the tranfer curve (drain current in red and gate current in grey) as a function of the applied gate bias (V_{DS}=3 mV). c. Current (V_{DS}=1 V) normalized*

by its value at room temperature as a function of the temperature for an array of HgTe NCs. d. Dark I-V curve, at room temperature, for the HgTe NCs array. The inset is the transfer curve as a function of applied gate bias (V_{DS}=100 mV). Parts c and d are measured on gold interdigitated electrodes. e. Current (V_{DS}=1 V) normalized by its value at room temperature, as a function of the temperature for the hybrid structure made of the InGaAs wires (connected to only one end) coated by an HgTe NCs film. f. Dark I-V curves, at various temperatures, for the hybrid structure.

Once the p-type HgTe NC array is deposited on the n-type wire array, a diode is formed as evidenced by the strongly rectifying I-V curve obtained, see **Figure 2**f. At 200 K, the current asymmetry reaches 3 orders of magnitude between the forward and reverse bias polarity, see **Figure 3**a. Another synergistic effect of the coupling between the two materials is observed from the temperature dependence of the current. The latter is strongly enhanced and the activation energy of the transport now reaches 400 meV, see **Figure 2**e. This increased activation makes the decrease of the dark current upon cooling even stronger.

We then focus on the photoconductive properties of the hybrid structure, see **Figure 3**. Under illumination we observe a current modulation, that is particularly large under reverse bias, **Figure 3**a. Unfortunately, the I-V curve under illumination does not present any open circuit voltage (V_{OC}). We attribute this lack of V_{OC} to the shunt resistance associated with the transport in NC along the wires. This can come from hole conduction beginning at the interface between the wire and the NCs up to the contact electrode and from a possible recombination of photogenerated carriers when the latter travel along the long n-type wires. This lack of V_{OC} prevents device operation under 0 V bias. However, with our strategy the dark current I-V curve is strongly rectifying and low dark current is maintained even under large negative reverse bias (even at -4 V). It contrasts with most diodes based on HgTe NCs[24–30] in which the current asymmetry is generally lost above 0.4 V.

Photocurrent spectroscopy is then used to understand the origin of the photocarriers, see **Figure 3**b. Just below 1 µm, the intense peak comes from the InP substrate. In the SWIR region, we observe an absorption signal that matches the HgTe NCs absorption. No feature from the InGaAs is observed. Moreover, the photocurrent is unpolarized. To understand these properties, we have simulated the absorption map and spectrum of the hybrid structure with a finite element commercial tool (see method), **Figure 3**e-f and S2-3. Even though it is intense below the band gap of InGaAs (**Figure 3**e), the absorption of the III-V material only accounts for a small volume of the total structure. As a result, the absorption occurring within the InGaAs only accounts for a few % of the total absorption, see **Figure 3**d. In other words, in this hybrid structure the roles are clearly split between both materials. The HgTe NCs film drives the absorption, while the InGaAs drives the transport and behaves as a unipolar barrier extracting the generated photoelectrons. The weak absorption from the InGaAs also explains why the total absorption is not polarized despite of the oriented wires structure, see **Figure 3**c. This simple strategy expands the spectral response of the InGaAs by 400 nm (from 1.6 to 2 µm cut-off wavelength), see **Figure 3**d and S2-3.

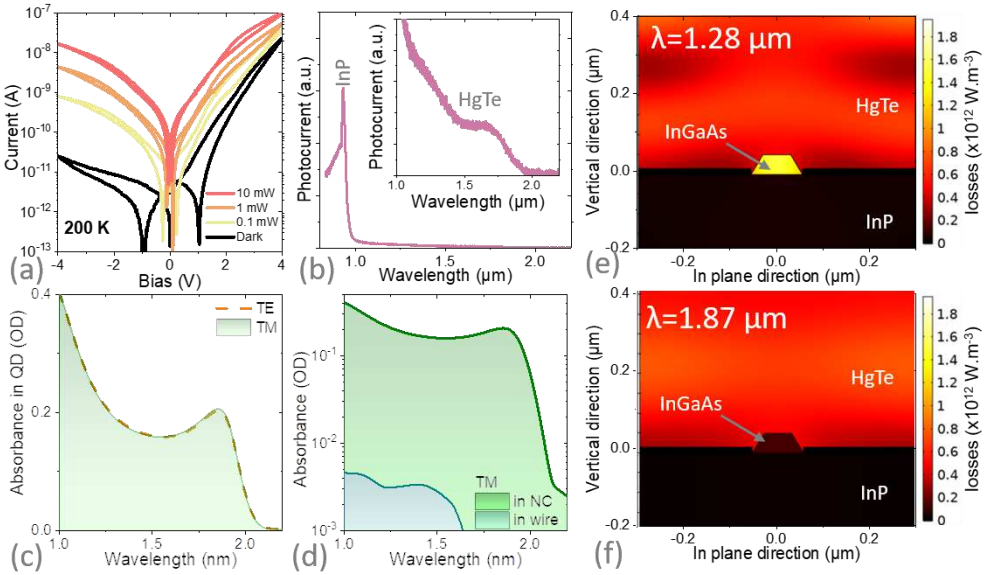

Figure 3 Spectroscopic properties of the photocurrent*. a. I-V curves of the hybrid structure in the dark and under illumination by a laser diode (λ=1.55 μm). The indicated power is the one from the laser diode. b. Photocurrent spectrum for the hybrid structure. The inset is a zoom on the spectral range corresponding to the band edge of HgTe. c. Simulated absorption of the hybrid structure along the TE and TM polarization. d. Simulated absorption of the hybrid structure along the TM polarization (Figure S1 for TE) within the InGaAs wires and within the HgTe NCs. e. Absorption map of the hybrid structure at 1.28 μm (below InGaAs band gap). f. Aborption map of the hybrid structure at 1.87 μm (above InGaAs band gap). Maps from part e and f are simulated in TE polarization.*

Finally, we quantify the performance of this diode for IR sensing. Under illumination, the responsivity appears to be proportional to the applied bias. The responsivity magnitude is weakly dependent of the bias sign, see **Figure 4**a and reaches 16 $mA.W^{-1}$ at -4 V. Since the dark I-V curve is, on the other hand, strongly dependent of the bias polarity, the optimal operating condition (*i.e.,* the one leading to the largest current modulation) appears to be under large (-4 V) reverse bias for this diode. Upon cooling from 300 to 200 K the responsivity is reduced by a factor 2 (**Figure 4**b), while the dark current drops by three orders of magnitude. In the nanocrystal array, the charge conduction is occurring though hopping mechanism. The latter leads to thermal activation of both carrier density and mobility. Under illumination the carrier density is set by the incident photon flux and thus the temperature dependence of the response is mostly the result of the thermal activation of the carrier mobility.

Finally, the responsivity depends on the incident photon flux (photocurrent scales as $P^{0.63}$, with P the incident power) and larger responses are measured under weaker irradiations, see **Figure 4**c.

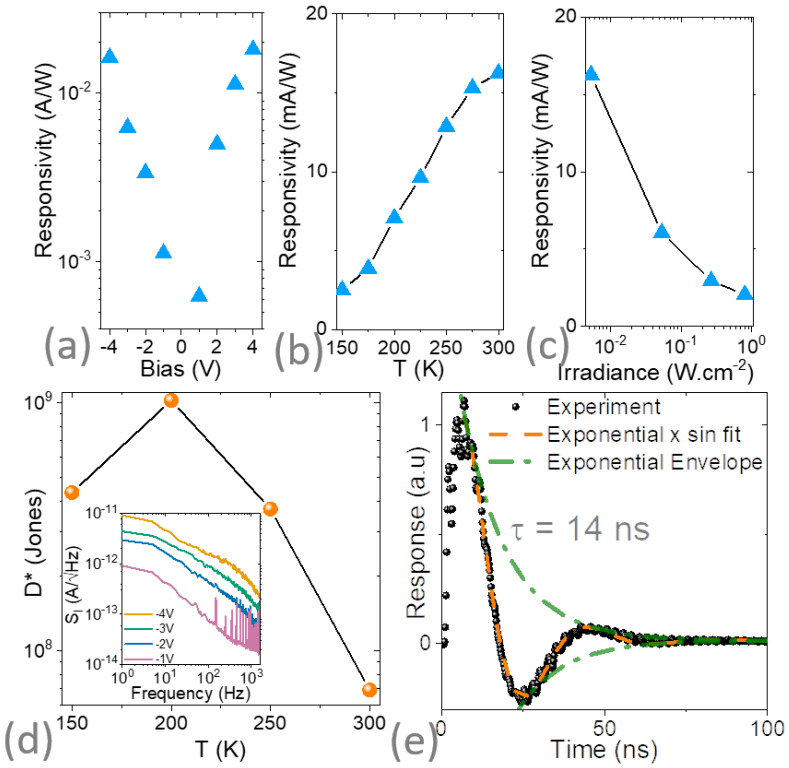

Figure 4 Photodetection performance of the hybrid structure. *a. Responsivity at 300 K of the hybrid structure as a function of the applied bias, under illumination by a laser diode at 1.55 µm with an irradiance of 5x10^{-3} W.cm^{-2}. b. Responsivity of the hybrid structure as a function of the temperature, under -4 V under an irradiance of 5x10^{-3} W.cm^{-2} at 1.55 µm. c. Responsivity of the hybrid structure as a function of the incident irradiance power, at 300 K under -4 V. d. Specific detectivity under -4 V as a function of the operating temperature for a signal modulated at 1 kHz. The inset is the noise current spectral density as a function of the signal frequency, while the device is operated under various biases. e. Photocurrent response of the hybrid structure to a 1 ns pulse of light at 1.57 µm. The data are fitted by the product of an exponential decay curve with a sinus curve accounting for the unperfectly impedance matching of the device with the acquisition scope. Exponential decay time is estimated to be ≈14 ns.*

The noise in the structure appears to be *1/f* limited, see the inset of **Figure 4**d. This suggests that the noise is mostly coming from the transport in the NC array,[31] since charge conduction in high mobility III-V semiconductor films is generally associated with white noise only (shot and thermal noises). The detectivity of the diode is 7x10^{7} jones at room T and reaches 10^{9} jones at 200 K and under -4 V for a 2 µm cut-off wavelength and for a signal modulated at 1 kHz. This is weaker than state-of-the-art diodes based on HgTe NCs. At similar wavelengths, those diodes achieve detectivity up to 10^{10}-10^{11} jones at room temperature.[28,32,33] But the achieved detectivity is similar to the one reported for HgTe NC layer coupled to graphene for which detectivity are in the 10^{8}-10^{9} jones range.[16,34] Certainly, our approach suffers from the lack of V_{OC} preventing the zero volt operation. On the other hand, thanks to its planar geometry, that is associated with a weaker capacitance than the vertical geometry diode, fast operation can be achieved. Under illumination by a 1 ns pulse at

1.57 µm, our device shows an exponential decay of the signal with a characteristic decay time of 14 ns, see **Figure 4**e. This is two orders of magnitude faster than the value reported for the vertical diodes.[28] In this sense, the weaker signal-to-noise ratio is balanced by a higher device bandwidth.

For a long time, the design of IR sensors has opposed narrow band gap III-V semiconductors against their colloidal II-VI counterpart. Here we demonstrate that Van der Walls heterostructures can be obtained from these two types of semiconductors. We propose a geometry where high mobility *n*-type InGaAs wires are used as electron extractors from a *p*-type HgTe NCs array. Our device tackles the belief that such designs are limited to graphene-like materials with nanocrystals acting as light sensitizers on top. Epitaxially and colloidally grown semiconductors can combine their advantages: this approach has been conveniently applied to expand the spectral response of the InGaAs technology toward longer wavelengths, while waiving all epitaxial growth constraints. The achieved performances ($R>10$ mA.W^{-1}, $D^*>10^9$ jones at 200 K, 14 ns decay time) paves the way to further the explore this hybrid device combining epitaxially grown and colloidally grown materials. The next challenge will be to combine the architecture with gate control and light management to further enhanced the signal to noise ratio

SUPPORTING INFORMATION

Supporting Information include details about fabrication of the device, additional electromagnetic simulation and setup for device characterization

ACKNOWLEDEGMENTS

The project is supported by ERC starting grant blackQD (grant n° 756225). We acknowledge the use of clean-room facilities from the "Centrale de Proximité Paris-Centre". This work has been supported by the Region Ile-de-France in the framework of DIM Nano-K (grant dopQD). This work was supported by French state funds managed by the ANR within the Investissements d'Avenir programme under reference ANR-11-IDEX-0004-02, and more specifically within the framework of the Cluster of Excellence MATISSE and also by the grant IPER-Nano2 (ANR-18CE30-0023-01), Copin (ANR-19-CE24-0022), Frontal (ANR-19-CE09-0017), Graskop (ANR-19-CE09-0026), NITQuantum (ANR-20-ASTR-0008-01), Bright (ANR-21-CE24-0012-02) and MixDFerro (ANR-21-CE09-0029.). This work was partly supported by the French Renatech network.

CONFLICT OF INTEREST

The authors declare no competing financial interest.

Keywords: InGaAs, HgTe, nanowire, quantum dot, short wave infrared, light sensing, photodiode

REFERENCES

[1] G.H. Carey, A.L. Abdelhady, Z. Ning, S.M. Thon, O.M. Bakr, and E.H. Sargent, Chem. Rev. **115**, 12732 (2015).
[2] T. Rauch, M. Böberl, S.F. Tedde, J. Fürst, M.V. Kovalenko, G. Hesser, U. Lemmer, W. Heiss, and O. Hayden, Nat. Photonics **3**, 332 (2009).
[3] J. Lee, E. Georgitzikis, Y. Li, Z. Lin, J. Park, I. Lieberman, D. Cheyns, M. Jayapala, A. Lambrechts, S. Thijs, R. Stahl, and P.E. Malinowski, in *2020 IEEE Int. Electron Devices Meet. IEDM* (2020), p. 16.5.1-16.5.4.
[4] A. Chu, B. Martinez, S. Ferré, V. Noguier, C. Gréboval, C. Livache, J. Qu, Y. Prado, N. Casaretto, N. Goubet, H. Cruguel, L. Dudy, M.G. Silly, G. Vincent, and E. Lhuillier, ACS Appl. Mater. Interfaces **11**, 33116 (2019).
[5] A.J. Ciani, R.E. Pimpinella, C.H. Grein, and P. Guyot-Sionnest, in *Infrared Technol. Appl. XLII* (SPIE, 2016), pp. 333–341.
[6] A. Rogalski and R. Ciupa, J. Electron. Mater. **28**, 630 (1999).
[7] A. Bucamp, C. Coinon, J.-L. Codron, D. Troadec, X. Wallart, and L. Desplanque, J. Cryst. Growth **512**, 11 (2019).
[8] J. Jean, S. Chang, P.R. Brown, J.J. Cheng, P.H. Rekemeyer, M.G. Bawendi, S. Gradečak, and V. Bulović, Adv. Mater. **25**, 2790 (2013).
[9] M. Law, L.E. Greene, J.C. Johnson, R. Saykally, and P. Yang, Nat. Mater. **4**, 455 (2005).
[10] A. Jagtap, N. Goubet, C. Livache, A. Chu, B. Martinez, C. Gréboval, J. Qu, E. Dandeu, L. Becerra, N. Witkowski, S. Ithurria, F. Mathevet, M.G. Silly, B. Dubertret, and E. Lhuillier, J. Phys. Chem. C **122**, 14979 (2018).
[11] D. Jariwala, T.J. Marks, and M.C. Hersam, Nat. Mater. **16**, 170 (2017).
[12] A.K. Geim and I.V. Grigorieva, Nature **499**, 419 (2013).
[13] H. Henck, Z. Ben Aziza, D. Pierucci, F. Laourine, F. Reale, P. Palczynski, J. Chaste, M.G. Silly, F. Bertran, P. Le Fèvre, E. Lhuillier, T. Wakamura, C. Mattevi, J.E. Rault, M. Calandra, and A. Ouerghi, Phys. Rev. B **97**, 155421 (2018).
[14] L. Khalil, D. Pierucci, E. Papalazarou, J. Chaste, M.G. Silly, F. Sirotti, M. Eddrief, L. Perfetti, E. Lhuillier, and A. Ouerghi, Phys. Rev. Mater. **3**, 084002 (2019).
[15] G. Konstantatos, M. Badioli, L. Gaudreau, J. Osmond, M. Bernechea, F.P.G. de Arquer, F. Gatti, and F.H.L. Koppens, Nat. Nanotechnol. **7**, 363 (2012).
[16] U.N. Noumbé, C. Gréboval, C. Livache, A. Chu, H. Majjad, L.E. Parra López, L.D.N. Mouafo, B. Doudin, S. Berciaud, J. Chaste, A. Ouerghi, E. Lhuillier, and J.-F. Dayen, ACS Nano **14**, 4567 (2020).
[17] H. Henck, Z. Ben Aziza, O. Zill, D. Pierucci, C.H. Naylor, M.G. Silly, N. Gogneau, F. Oehler, S. Collin, J. Brault, F. Sirotti, F. Bertran, P. Le Fèvre, S. Berciaud, A.T.C. Johnson, E. Lhuillier, J.E. Rault, and A. Ouerghi, Phys. Rev. B **96**, 115312 (2017).
[18] S. Masala, V. Adinolfi, J.-P. Sun, S.D. Gobbo, O. Voznyy, I.J. Kramer, I.G. Hill, and E.H. Sargent, Adv. Mater. **27**, 7445 (2015).
[19] A. Jagtap, B. Martinez, N. Goubet, A. Chu, C. Livache, C. Gréboval, J. Ramade, D. Amelot, P. Trousset, A. Triboulin, S. Ithurria, M.G. Silly, B. Dubertret, and E. Lhuillier, ACS Photonics **5**, 4569 (2018).
[20] M.M. Ackerman, X. Tang, and P. Guyot-Sionnest, ACS Nano **12**, 7264 (2018).
[21] C.-H.M. Chuang, P.R. Brown, V. Bulović, and M.G. Bawendi, Nat. Mater. **13**, 796 (2014).
[22] C. Gréboval, A. Chu, N. Goubet, C. Livache, S. Ithurria, and E. Lhuillier, Chem. Rev. **121**, 3627 (2021).
[23] S. Keuleyan, E. Lhuillier, and P. Guyot-Sionnest, J. Am. Chem. Soc. **133**, 16422 (2011).
[24] C. Gréboval, U.N. Noumbé, A. Chu, Y. Prado, A. Khalili, C. Dabard, T.H. Dang, S. Colis, J. Chaste, A. Ouerghi, J.-F. Dayen, and E. Lhuillier, Appl. Phys. Lett. **117**, 251104 (2020).
[25] S.-S. Chee, C. Gréboval, D.V. Magalhaes, J. Ramade, A. Chu, J. Qu, P. Rastogi, A. Khalili, T.H. Dang, C. Dabard, Y. Prado, G. Patriarche, J. Chaste, M. Rosticher, S. Bals, C. Delerue, and E. Lhuillier, Nano Lett. **21**, 4145 (2021).
[26] P. Rastogi, A. Chu, T.H. Dang, Y. Prado, C. Gréboval, J. Qu, C. Dabard, A. Khalili, E. Dandeu, B. Fix, X.Z. Xu, S. Ithurria, G. Vincent, B. Gallas, and E. Lhuillier, Adv. Opt. Mater. **9**, 2002066 (2021).

[27] B. Martinez, J. Ramade, C. Livache, N. Goubet, A. Chu, C. Gréboval, J. Qu, W.L. Watkins, L. Becerra, E. Dandeu, J.L. Fave, C. Méthivier, E. Lacaze, and E. Lhuillier, Adv. Opt. Mater. **7**, 1900348 (2019).
[28] M.M. Ackerman, M. Chen, and P. Guyot-Sionnest, Appl. Phys. Lett. **116**, 083502 (2020).
[29] X. Tang, M.M. Ackerman, G. Shen, and P. Guyot-Sionnest, Small **15**, 1804920 (2019).
[30] M. Chen, L. Shao, S.V. Kershaw, H. Yu, J. Wang, A.L. Rogach, and N. Zhao, ACS Nano **8**, 8208 (2014).
[31] H. Liu, E. Lhuillier, and P. Guyot-Sionnest, J. Appl. Phys. **115**, 154309 (2014).
[32] Y. Dong, M. Chen, W.K. Yiu, Q. Zhu, G. Zhou, S.V. Kershaw, N. Ke, C.P. Wong, A.L. Rogach, and N. Zhao, Adv. Sci. **7**, 2000068 (2020).
[33] A. Chu, C. Gréboval, Y. Prado, H. Majjad, C. Delerue, J.-F. Dayen, G. Vincent, and E. Lhuillier, Nat. Commun. **12**, 1794 (2021).
[34] M.J. Grotevent, C.U. Hail, S. Yakunin, D. Bachmann, M. Calame, D. Poulikakos, M.V. Kovalenko, and I. Shorubalko, Adv. Sci. **8**, 2003360 (2021).

PLEASE CITE THIS ARTICLE AS DOI: 10.1063/5.0076708